energies

MDPI

Article

Integrated Design and Dynamic Response Analysis of the EV Reducer Considering Mass Eccentricity

Yuan Guan [1], Yao Li [1,*], Yue Deng [1], Gaoxiang Ni [1], Zifan Fang [1] and Dong Huang [2]

[1] College of Mechanical & Power, China Three Gorges University, Yichang 443002, China; 202208550021014@ctgu.edu.cn (Y.G.)
[2] Department of Technology, Chongqing Tsingshan Industrial Co., Ltd., Chongqing 402776, China
* Correspondence: yao_li_@outlook.com

Abstract: To meet the high-performance demands of electric vehicle reducers, the authors present a novel approach for parameter matching in electric drive systems for electric vehicles. Based on fuzzy evaluation, the method identifies the optimal performance parameters for the entire vehicle and determines the best transmission ratio scheme for the reducer. The gear geometrical parameters of the reducer are derived using the transmission ratio scheme as the constraint condition. An 18-degree-of-freedom dynamic system model, incorporating factors such as time-varying mesh stiffness, the backlash, time-varying transmission error and mass eccentricity, has been built using Matlab. The dynamic response of the gear system under the designed gear parameter scheme have been analyzed and compared with the gear parameter results obtained using KISSsoft, demonstrating the accuracy and rigour of the design. This research has practical implications for the design and performance optimization of electric vehicle reducers.

Keywords: parameter matching; gear design; nonlinear dynamics; mass eccentricity

check for updates

Academic Editor: Giovanni Lutzemberger

Received: 18 December 2024
Revised: 16 January 2025
Accepted: 17 January 2025
Published: 24 January 2025

Citation: Guan, Y.; Li, Y.; Deng, Y.; Ni, G.; Fang, Z.; Huang, D. Integrated Design and Dynamic Response Analysis of the EV Reducer Considering Mass Eccentricity. *Energies* **2025**, *18*, 530. https://doi.org/10.3390/en18030530

Copyright: © 2025 by the authors. Licensee MDPI, Basel, Switzerland. This article is an open access article distributed under the terms and conditions of the Creative Commons Attribution (CC BY) license (https://creativecommons.org/licenses/by/4.0/).

1. Introduction

Nowadays, electric vehicles (EV) have become a research hotspot in the field of new energy vehicles due to their advantages of energy saving and environmental protection [1,2]. The driving system of pure electric vehicles has the distinctive characteristics of high torque and speed. It is crucial to consider the parameter matching and geometric parameter design of the reducer, which should comprehensively consider vehicle dynamics and economy [3]. Based on the obtained optimal transmission ratio, reasonable transmission ratio distribution and gear geometry parameter design are the keys to ensuring the comprehensive performance of electric vehicles.

The parameter matching, design, and analysis of electric vehicle reducers have been extensively studied. Gao et al. [4] proposed a two-stage multi-objective optimization method that considers structural parameters and modifications to achieve high transmission efficiency and a small reducer size. Moya et al. [5] proposed a design method for compact reducers for electric vehicles taking into account mass and energy consumption. Wang et al. [6] proposed an integrated transmission scheme for electric vehicle reducers and obtained relatively optimal design parameters. Zhao et al. [7] used an improved parallel adaptive genetic algorithm to solve and obtain the optimal design solution. Maradona et al. [8] proposed a highly efficient and effective gear optimization design method. Hur et al. [9] performed the optimization design for the compound planetary reducers using the Sequential Least Squares Programming method. Trojovská et al. [10] proposed the Zebra Optimisation Algorithm for solving real-world engineering problems

based on a mathematical model. However, a strong coupling between system parameters and comprehensive performance makes it difficult to optimize these objectives simultaneously. Determining which scheme is the best match under unrestricted conditions is difficult in engineering practice. Fuzzy evaluation is used in several fields as an excellent evaluation method [11,12]. Therefore, this paper proposes a new parameter-matching method for electric drive systems of electric vehicles based on the fuzzy evaluation. It comprehensively considers the entire vehicle's power and economy, which can significantly shorten the parameter-matching time and improve the accuracy of transmission ratio matching.

For the dynamic response analysis of the reducer, Khabou et al. [13] studied the dynamic response of a single-stage gear reducer under transient conditions. Lin et al. [14] established the corresponding motion differential equations based on Newton's laws of motion and investigated a rear-wheel-drive electric vehicle with a manual transmission. Guo et al. [15] established a multi-bearing collaborative pre-tightening dynamic model for an electric vehicle reducer. Al-Tayari et al. [16] developed a coupled nonlinear dynamic model for an electric vehicle reducer and studied the effects of pinion parameters on the system's dynamic response. Yan et al. [17] studied the calculation method for relative displacement along the line of action. Chen et al. [18] developed an improved dynamic model of the spur gear pair that considered teeth deformations. Kong et al. [19] proposed a dynamic modelling method that could consider gear flexibility, the results of which were verified. Huang et al. [20] analysed the bifurcation and chaotic behaviour of a spur gear pair system with a fractal backlash, and investigated the effects of different initial backlash and rotational speeds on the dynamical characteristics of the system. Guan et al. [21] established a dynamic model of a lightweight spur gear transmission system considering the elasticity of the shaft and the gear body, and investigated the effect of the elasticity of the gear body on the dynamic characteristics of the system. However, most research focused on establishing dynamic equations for gear meshing and bearing support while ignoring the influences of gear shaft flexibility and mass eccentricity on the system's dynamic behaviour. This paper develops a non-linear dynamic model with an 18-degree-of-freedom for the two-stage helical gear transmission system, which considers the backlash, real-time transmission error of meshing, and gear mass eccentricity.

As can be seen from the above literature, parameter matching needs to consider the whole vehicle's parameters and performance to avoid significant errors. There is a strong coupling relationship between vehicle parameters and parameter matching through a single performance. Conventional optimization methods can easily result in a local optimal solution rather than a global optimal solution, which further affects the subsequent design process and results in the inability to obtain better reducer geometric parameters. Therefore, we proposed a reducer parameter matching method to obtain the optimal reducer transmission ratio and the reducer geometric parameters. The method is based on analysing the simulation performance of the whole vehicle and selecting the transmission ratio scheme inversely, which achieves ensuring the optimal performance and effectively avoids the problem of locally optimal solution caused by using traditional algorithms. Following this, a nonlinear dynamic model of the EV reducer was established based on the designed reducer geometric parameters, and the dynamic behavior of the transmission system was studied. The rest of this paper is organized as follows. Section 2 proposes the parameter matching method based on fuzzy evaluation for the EVs. Section 3 performs the geometric parameter design for the EV reducer's gear transmission. Section 4 shows the dynamic model of the reducer using the Lumped Parameter Method. Following this, Section 4.2 presents the dynamic response analysis and discussion. Section 5 summarises some conclusions of this article.

2. Fuzzy Evaluation Based Parameter Matching Method of the EV Reducer

To obtain the optimal geomereic parameter and comprehensive performance of the EV reducer, this study built a parameter matching model considering the multi-dimensional performance indicators.

2.1. Multi-Dimensional Evaluation Indicators

To ensure the authority of the fuzzy comprehensive evaluation method, multiple evaluation indicators are selected to develop the comprehensive evaluation system. The comprehensive performance of the EV can be evaluated in two dimensions: power performance and economic performance. The power performance includes the following indicators: 0∼100 km/h acceleration time (A_1), 40∼80 km/h acceleration time (A_2), 80∼120 km/h acceleration time (A_3), maximum gradient climb (A_4), and maximum speed (A_5). The economic performance is quantified by the 100 km electric power consumption in WLTC working conditions (A_6). Subsequently, the weights are assigned to each dimension indicator. The matrix system to be evaluated is defined as:

$$T = [A_1, A_2, A_3, A_4, A_5, A_6] \tag{1}$$

2.2. Parameter Matching Modelling Based on Fuzzy Evaluation

The simulation model of the whole vehicle is built as shown in Figure 1, and the simulation data of the EV under different transmission ratios are extracted and analysed [22]. The original index matrix can be obtained based on the simulation data. Equation (2) is used to standardize the original indicator matrix.

$$y_{ij}{}' = \frac{y_{ij}}{\sqrt{\sum_{i=1}^{m} y_{ij}{}^2}} \quad (i = 1, 2, \cdots, m; j = 1, 2, \cdots, n) \tag{2}$$

where y_{ij} represents the raw data under each performance metric.

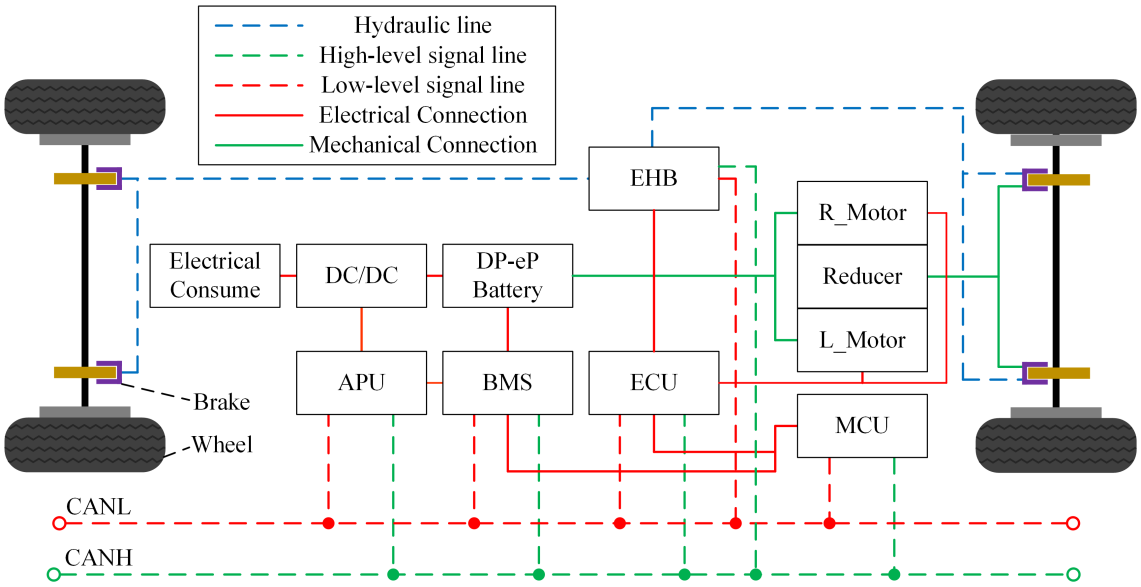

Figure 1. The simulation model of the whole vehicle.

According to the obtained standardized matrix, combined with the performance data and design experience of EVs, the evaluation indicators of the whole vehicle are divided into five levels: very low, low, general, high, and very high. The thresholds of the whole vehicle performance at different levels are set.

In order to obtain a single-factor evaluation set with high fidelity, the initial evaluation index matrix is analyzed using triangular fuzzy analysis. The calculation formula of the evaluation set of the kth design scheme can be expressed as:

$$R_k = \begin{array}{c} \text{index} \\ X_1 \\ X_2 \\ \vdots \\ X_6 \end{array} \begin{bmatrix} V_{vl} & V_l & V_n & V_h & V_{vh} \\ \tilde{p}_{1,1} & \tilde{p}_{1,2} & \tilde{p}_{1,3} & \tilde{p}_{1,4} & \tilde{p}_{1,5} \\ \tilde{p}_{2,1} & \tilde{p}_{2,2} & \tilde{p}_{2,3} & \tilde{p}_{2,4} & \tilde{p}_{2,5} \\ \vdots & \vdots & \vdots & \vdots & \vdots \\ \tilde{p}_{6,1} & \tilde{p}_{6,2} & \tilde{p}_{6,3} & \tilde{p}_{6,4} & \tilde{p}_{6,5} \end{bmatrix} \tag{3}$$

where $\tilde{p}_{i,j}$ denotes the membership degree of the indictor X_i in the evaluation set with respect to the performance level V_j. The membership degree ($\tilde{p}_{i,j}$) can be obtained by fuzzy mathematical method. This article employs the triangular fuzzy function, and $\tilde{p}_{i,j}$ can be calculated using the following formula

$$f(X_i) = \begin{cases} 1 & \text{if } X_i \le X_1 \\ \frac{x_2 - x_i}{x_2 - x_1} & \text{if } X_1 < X_i \le X_2 \\ \left(\frac{x_3 - x_i}{x_3 - x_2}, \frac{x_i - x_2}{x_2 - x_3} \right) & \text{if } X_2 < X_i \le X_3 \\ \vdots & \\ \frac{x_i - x_{m-1}}{x_m - x_{m-1}} & \text{if } X_{m-1} < X_i \le X_m \\ 1 & \text{if } X_m < X_i \end{cases} \tag{4}$$

where X_g ($g = 1, 2, ..., X_{m-1}, X_m$) represents the threshold for each evaluation level, x_h ($h = 1, 2, ..., x_{m-1}, x_m$) represents the triangular fuzzy function affiliation at the threshold of each evaluation level.

For a multi-state system with m states and n evaluation indicators, assuming that the original evaluation indicator matrix is $\mathbf{Y} = [y_{ij}]_{m \times n}$, the information entropy for the jth indicator is

$$H_j^{fh} = -\sum_{i=1}^{m} f_{hi} \cdot \ln f_{hi} \tag{5}$$

where $f_{hi} = \sum_{j=1}^{m} p_{ij}/n$, p_{ij} represents the proportion of the ith state indicator under the jth indicator, which can be obtained by $p_{ij} = y_{ij} / \sum_{j=1}^{m} y_{ij}$, n represents the number of columns of the original evaluation indicator matrix.

The entropy weight matrix and the expert evaluation matrix are weighted comprehensively. The initial step is to define the entropy weight matrix ($\mathbf{W}_\mathrm{H}$), denoted as follows:

$$\mathbf{W}_\mathrm{H} = [w_{H1}, w_{H2}, \cdots, w_{Hn}] \tag{6}$$

where the entropy weight w_{Hj} of the jth indicator can be expressed as

$$w_{Hj} = \frac{1 - H_j^{fh}}{\sum_{j=1}^{n} \left(1 - H_j^{fh}\right)} \tag{7}$$

Then, comprehensively based on previous experimental data and expert evaluation experience, the Delphi method was used to set the expert evaluation matrix as

$$\mathbf{W}_z = [w_{z1}, w_{z2}, \cdots, w_{zn}] \tag{8}$$

Following this, the compound weight matrix $\mathbf{W}$ can be obtained by combining the entropy weight matrix and the expert evaluation matrix, which is shown as follows:

$$\mathbf{W} = [w_1, w_2, \cdots, w_n] \tag{9}$$

where $w_j = (w_{Hj} \cdot w_{zj}) / \sum_{j=1}^{n} w_{Hj} w_{zj}, j = 1, 2, \cdots, n$.

Combined with the single-factor evaluation matrix and the compound weights, the unit's evaluation matrix of the system can be obtained, as shown in Equation (10).

$$\mathbf{T}_k = [w_1, w_2, \cdots, w_n]\mathbf{M}(\cdot, \oplus) \begin{bmatrix} \tilde{p}_{1,1} & \tilde{p}_{1,2} & \cdots & \tilde{p}_{1,m} \\ \tilde{p}_{2,1} & \tilde{p}_{2,2} & \cdots & \tilde{p}_{2,m} \\ \vdots & \vdots & \ddots & \vdots \\ \tilde{p}_{n,1} & \tilde{p}_{n,2} & \cdots & \tilde{p}_{n,m} \end{bmatrix} \tag{10}$$

where $\mathbf{M}(\cdot, \oplus)$ is the fuzzy operator, and $k = 1, 2, \cdots, 6$.

According to the obtained vehicle comprehensive performance evaluation matrix, the evaluation level of the vehicle comprehensive performance under different transmission ratios is analyzed according to the maximum membership principle to achieve drive system parameter matching with the optimal comprehensive performance of the whole vehicle. The vehicle parameter matching model based on the fuzzy evaluation method is shown in Figure 2.

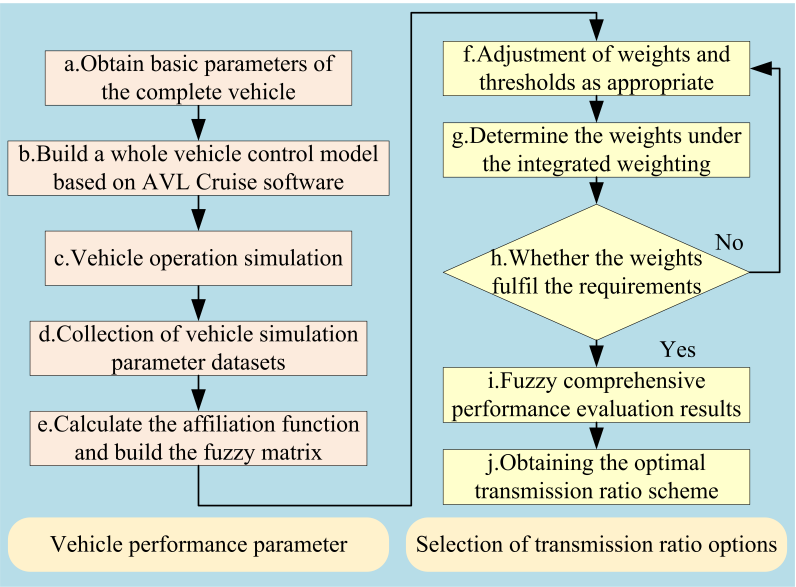

Figure 2. Parameter matching model for the EV.

2.3. Transmission Ratio Matching of the EV Reducer

Based on the built parameter matching model, a pure EV is selected to perform the transmission ratio matching of the EV reducer. The parameters of the whole EV is given in Table 1.

Table 1. Basic parameters of the vehicle.

Parameter	Value	Parameter	Value
Total weight/kg	2200	Distance from hitch to front axle/m	2.90
Curb weight/kg	1825	Height of support point/m	0.10
Front section/m^2	2.38	Aerodynamic drag factor	0.23
Rolling resistance	0.012	Motor's peak power/kW	129
Wheel base/m	2.90	Motor's rated voltage/V	400
Wheel radius/m	0.343	Motor's peak rotation/rpm	1000
Transmission efficiency	0.95	Motor's peak torque/N·m	326

According to the vehicle parameters and the method proposed in Section 2.2, the reducer's transmission ratio matching is performed, and the vehicle's performance indicators at different transmission ratios i_t are obtained, as shown in Figure 3.

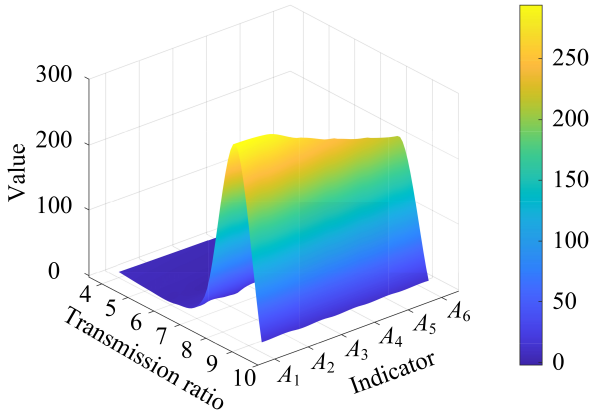

Figure 3. Performance indicators under different transmission ratios.

According to the simulation results and design requirements of new energy vehicles, the evaluation indexes of the vehicle are divided into five levels: Very Low, Low, Normal, High and Very high. The simulation results are evaluated using the fuzzy evaluation method and maximum membership principle. The comprehensive performance levels of the vehicle under different transmission ratios are obtained by combining the entropy weights and thresholds. It can be seen from Figure 4 that when the transmission ratio is 7.0, the comprehensive performance of the vehicle is "Very high" and the membership degree is the largest.

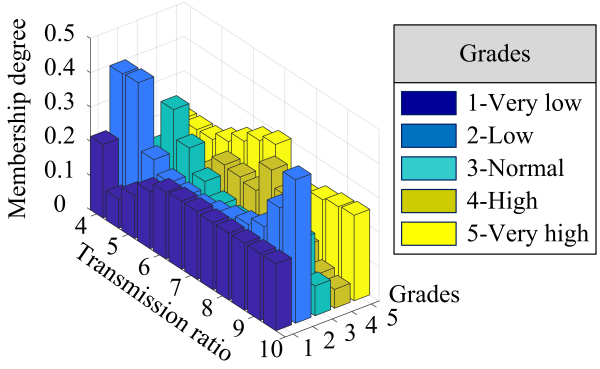

Figure 4. Vehicle's comprehensive performance evaluation matrix with ratios [4.0,9.5].

In order to obtain the optimal transmission ratio, we need to perform the reducer's transmission ratio matching between 6.5 and 7.5 again. The EV reducer's transmission ratio matching results are given in Figure 5. The results of Figure 5 shows that the transmission ratio with the maximum membership is 0.9. Therefore, the vehicle has the best comprehensive performance when the reducer transmission ratio is 0.9.

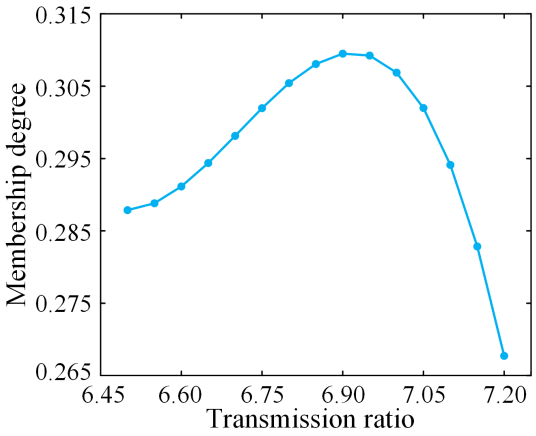

Figure 5. Membership degree of the matching results.

3. Geometric Parameter Design of the EV Reducer

The reducer's geometric parameters are designed according to the vehicle parameters, transmission ratio, and boundary conditions. The design process of the parallel shaft gear transmission system of the EV reducer is shown in Figure 6.

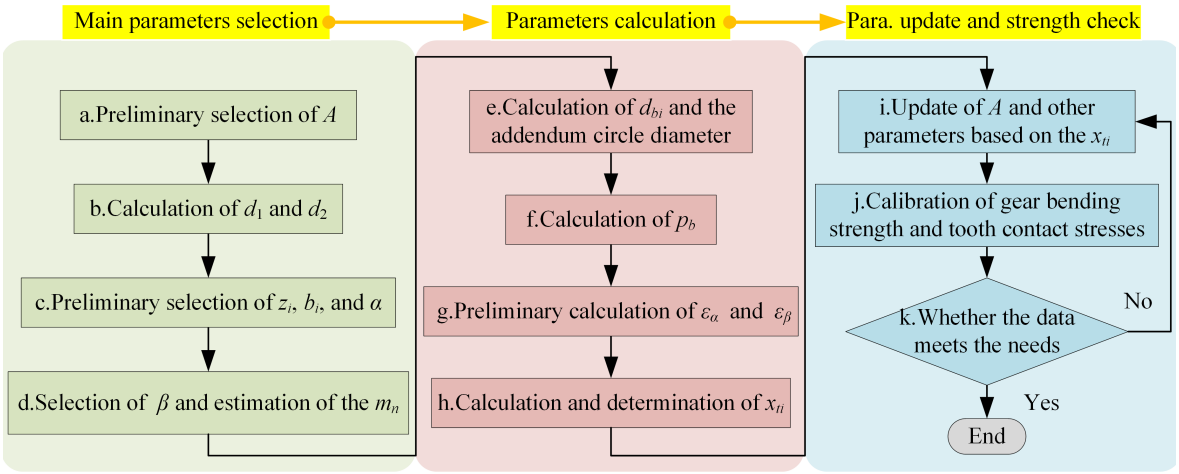

Figure 6. Flowchart of reducer's geometric parameter design.

The centre distance is one of the most critical essential characteristic parameters for parallel-axis reducers. The larger the transmitted torque, the larger the centre distance, and the larger the reducer's size, volume, weight, and cost. Therefore, the centre distance is initially selected according to the following formula:

$$A = K_A(T_{i\max})^{1/3} \tag{11}$$

where K_A is the centre distance coefficient, K_A is the centre distance coefficient, and since the simulation model is a passenger car, K_A takes the value of 14.5, A represents the initial center distance, while $T_{i\max}$ denotes the maximum torque of the reducer input shaft.

Based on the transmission ratio of the input stage and the centre distance, the pitch circle diameter of the input stage gears can be preliminarily calculated by Equation (12).

$$d_1 = \frac{2A}{1 + i_1} \tag{12}$$

where d_1 represents the pitch diameter of the pinion gear, and i_1 denotes the gear ratio of the gear.

The helical angle is crucial to the gear's strength performance, vibration characteristics, and noise level. Increasing the helix angle can effectively improve the contact ratio, ensuring smooth operation and low noise of the gear pair. However, it also significantly increases axial force when it exceeds 30° and reduces the gear teeth' bending strength. Once the helical angle is preliminarily determined, the normal module can be calculated using Equation (13).

$$m_n = \frac{2A\cos\beta}{z_1 + z_2} \tag{13}$$

where m_n denotes the normal modulus of gears, β denotes the helix angle of the gear, and z_1 and z_2 denote the number of teeth of the input and output gears respectively.

Following this, the standard value of the helical angle can be obtained according to the estimated value of the normal module. The helical angle can be optimized based on the rounded normal module using Equation (14).

$$\beta = \frac{180}{\pi}\arccos\frac{m_n(z_1 + z_2)}{2A} \tag{14}$$

The pitch of the base circle is equal to $p_b = \frac{2\pi r_{b1}}{z_1}$. The updated value of the helical angle can be used to calculate the equivalent number of teeth (z_{v1}, z_{v2}) of the pinion and gear. The modification coefficients (x_{t1}, x_{t2}) are selected based on the standards. Following this, according to the equivalent number of teeth and the modification coefficients, the tooth root stress could be calculated with the tooth shape coefficient Y_F.

After the modification coefficient is determined, the design parameters must be updated according to the modification situation. The modification of working depth does not affect the centre distance, but the angular modification gear needs to update the centre distance. The updated centre distance can be obtained by:

$$A' = A\frac{\cos\alpha_t}{\cos\alpha_t'} = \frac{1}{2}m_t(z_1 + z_2)\frac{\cos\alpha_t}{\cos\alpha_t'} = \frac{1}{2}m_n(z_1 + z_2)\frac{\cos\alpha_t}{\cos\beta\cos\alpha_t'} \tag{15}$$

where α_t represent the end face pressure angle of the gear, α_t' denotes the end face meshing angle of the gear and m_t is the end face modulus. A' is the updated centre distance. From this, the centre distance variation coefficient y_t can be calculated by

$$y_t = \frac{A' - A}{m_n} \tag{16}$$

The design parameters of the gears can be updated through the centre distance. The transverse contact ratio ε_α and face contact ratio ε_β are calculated. Finally, the tooth bending strength and tooth surface contact stress are checked according to the updated gear design parameters. If the strength does not meet the requirements, the centre distance and other design parameters must be adjusted appropriately and recalculated until they meet the requirements.

The parameter design process of the above helical gears is programed and the gear design parameters are obtained with the transmission ratio obtained in Section 2.3,

which is shown in Table 2. To verify the accuracy of the design scheme, we adopt the professional gear design tool KISSsoft to perform the parameter design process with the same transmission ratio. The results of the gears calculated by KISSsoft software (https://www.kisssoft.com/en) are very close to the results of the gears we designed, which indirectly confirms the rigour of the gear design process.

Table 2. Gear parameters under the design calculation process.

Name	Gear 1	Gear 2	Gear 3	Gear 4
Number of teeth	19	46	21	61
Tooth width (mm)	44	39	46	41
Normal modulus (mm)	2.75		2.75	
Pressure angle (°)	20		20	
Helical angle (°)	35		30	
Rotation direction	R	L	L	R
Modification coefficient	0.12	0.108	0.191	0.132
Face contact ratio	1.26		1.54	
Transverse contact ratio	2.59		2.37	
Total contact ratio	3.85		3.91	
Centre distance (mm)	109.11		130.19	
Gear transmission ratio	2.42		2.54	

4. Dynamic Modeling and Analysis of the Reducer's Gear Transmission

4.1. Dynamic Modeling of the Gear Transmission with Mass Eccentricity

To verify the dynamic performance of the designed gear parameters, the nonlinear dynamic model of the EV gear transmission sytem with 18 degrees of freedom was built using the lumped mass method, as shown in Figure 7. The model includes four helical gears, numbered by 1, 2, 3, and 4. Each gear is represented as a rigid block with four degrees of freedom, including one rotational degree of freedom around the z axis and three translational degrees of freedom in the x, y, and z directions. The motion equations of the each gear can be written as:

For the driving end, the motion equations can be erxpressed as:

$$J_D\ddot{\theta}_D + c_{e1}(\dot{\theta}_D - \dot{\theta}_1) + k_{e1}(\theta_D - \theta_1) = T_D \tag{17}$$

For gear 1, the corresponding motion equations are expressed as:

$$\begin{aligned}
&m_1\ddot{x}_1 + c_{x1}\dot{x}_1 + k_{x1}x_1 = -F_{x1} + m_1\rho_1\ddot{\theta}_1\sin\varphi_1 + m_1\rho_1(\omega_1 + \dot{\theta}_1)^2\cos\varphi_1\\
&m_1\ddot{y}_1 + c_{y1}\dot{y}_1 + k_{y1}y_1 = -F_{y1} - m_1\rho_1\ddot{\theta}_1\sin\varphi_1 + m_1\rho_1(\omega_1 + \dot{\theta}_1)^2\sin\varphi_1 - m_1g\\
&m_1\ddot{z}_1 + c_{z1}\dot{z}_1 + k_{z1}y_1 = -F_{z1}\\
&(J_1 + m_1\rho_1^2)\ddot{\theta}_1 + c_{e1}(\dot{\theta}_1 - \dot{\theta}_D) + k_{e1}(\theta_1 - \theta_D) = m_1\rho_1\ddot{x}_1\sin\varphi_1 - m_1\rho_1\ddot{y}_1\cos\varphi_1\\
&\quad - F_{m1}r_{b1}
\end{aligned} \tag{18}$$

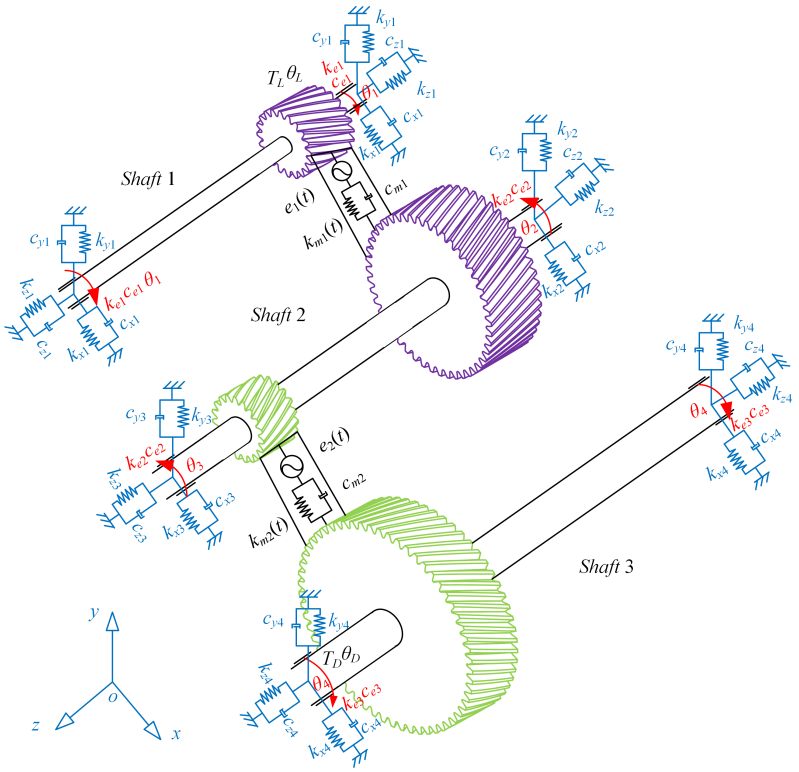

Figure 7. Dynamic model of the reducer's gear transmission system.

For gear 2, the corresponding motion equations are expressed as:

$$\begin{aligned}
&m_2\ddot{x}_2 + c_{x2}\dot{x}_2 + k_{x2}x_2 = F_{x2} + m_2\rho_2\ddot{\theta}_2\sin\varphi_2 + m_2\rho_2(\omega_2+\dot{\theta}_2)^2\cos\varphi_2\\
&m_2\ddot{y}_2 + c_{y2}\dot{y}_2 + k_{y2}y_2 = F_{y2} + m_2\rho_2\ddot{\theta}_2\sin\varphi_2 - m_2\rho_2(\omega_2+\dot{\theta}_2)^2\sin\varphi_2 - m_2g\\
&m_2\ddot{z}_2 + c_{z2}\dot{z}_2 + k_{z2}y_2 = F_{z2}\\
&\left(J_2 + m_2\rho_2^2\right)\ddot{\theta}_2 + c_{e2}(\dot{\theta}_2-\dot{\theta}_3) + k_{e2}(\theta_2-\theta_3) = m_2\rho_2\ddot{x}_2\sin\varphi_2 + m_2\rho_2\ddot{y}_2\cos\varphi_2\\
&\quad + F_{m2}r_{b2}
\end{aligned} \tag{19}$$

For gear 3, the corresponding motion equations are expressed as:

$$\begin{aligned}
&m_3\ddot{x}_3 + c_{x3}\dot{x}_3 + k_{x3}x_3 = -F_{x3} + m_3\rho_3\ddot{\theta}_3\sin\varphi_3 + m_3\rho_3(\omega_3+\dot{\theta}_3)^2\cos\varphi_3\\
&m_3\ddot{y}_3 + c_{y3}\dot{y}_3 + k_{y3}y_3 = -F_{y3} + m_3\rho_3\ddot{\theta}_3\sin\varphi_3 + m_3\rho_3(\omega_3+\dot{\theta}_3)^2\sin\varphi_3 - m_3g\\
&m_3\ddot{z}_3 + c_{z3}\dot{z}_3 + k_{z3}y_3 = -F_{z3}\\
&(J_3 + m_3\rho_3^2)\ddot{\theta}_3 + c_{e2}(\dot{\theta}_3-\dot{\theta}_2) + k_{e2}(\theta_3-\theta_2) = m_3\rho_3\ddot{x}_3\sin\varphi_3 - m_3\rho_3\ddot{y}_3\cos\varphi_3\\
&\quad - F_{m3}r_{b3}
\end{aligned} \tag{20}$$

For gear 4, the corresponding motion equations are expressed as:

$$\begin{aligned}
&m_4\ddot{x}_4 + c_{x4}\dot{x}_4 + k_{x4}x_4 = F_{x4} + m_4\rho_4\ddot{\theta}_4\sin\varphi_4 + m_4\rho_4(\omega_4+\dot{\theta}_4)^2\cos\varphi_4\\
&m_4\ddot{y}_4 + c_{y4}\dot{y}_4 + k_{y4}y_4 = F_{y4} + m_4\rho_4\ddot{\theta}_4\sin\varphi_4 - m_4\rho_4(\omega_4+\dot{\theta}_4)^2\sin\varphi_4 - m_4g\\
&m_4\dot{z}_4 + c_{z4}\ddot{z}_4 + k_{z4}y_4 = F_{z4}\\
&(J_4 + m_4\rho_4^2)\ddot{\theta}_4 + c_{e3}(\dot{\theta}_4-\dot{\theta}_L) + k_{e3}(\theta_4-\theta_L) = m_4\rho_4\ddot{x}_4\sin\varphi_4 + m_4\rho_4\ddot{y}_4\cos\varphi_4\\
&\quad + F_{m4}r_{b4}
\end{aligned} \tag{21}$$

For the driven end, the corresponding motion equations are expressed as:

$$J_L\ddot{\theta}_L + c_{e3}(\dot{\theta}_L - \dot{\theta}_4) + k_{e3}(\theta_L - \theta_4) = -T_L \tag{22}$$

where x_i, y_i, and z_i are the translational displacement of the corresponding gear along the x, y, and z axes; θ_i is the torsional displacement of the corresponding gear around the z axis (i = 1, 2, 3, 4). θ_D represents the torsional displacement of the driving end, θ_L is the torsional displacement of the driven end, m_i is the mass of the corresponding gear, k_{xi}, k_{yi}, and k_{zi} are the bending stiffness of the shaft along the x, y, and z directions, c_{xi}, c_{yi}, and c_{zi} are the bending damping of the shaft along the x, y, and z directions, k_{ei} is the torsional stiffness of the shaft, c_{ei} is the torsional damping of the shaft, J_i is the rotational inertia of the corresponding helical gear, J_D and J_L are the rotational inertia of the input and output ends, ρ_i means the gear mass eccentricity of the helical gear, φ_i is the rotation angle of the helical gear, r_{bi} is the base circle radius of the helical gear, F_{mi} is the dynamic meshing force between the teeth of the helical gear, F_{xi}, F_{yi}, and F_{zi} are the radial and axial components of the dynamic meshing force of each gear pair.

The generalized coordinate vector of the nonlinear dynamic model with 18 degrees of freedom can be defined as

$$\{q_m\} = \{\theta_D, x_1, y_1, z_1, \theta_1, x_2, y_2, z_2, \theta_2, x_3, y_3, z_3, \theta_3, x_4, y_4, z_4, \theta_4, \theta_L\}^T$$

The gear meshing stiffness can generally be represented as a Fourier series:

$$k_m(t) = k_p + \sum_{n=1}^{\infty} (a_n \cos(n\omega_m t + \varphi_n) + b_n \sin(n\omega_m t + \varphi_n)) \tag{23}$$

where k_p means the average value of the meshing stiffness, ω_m is the meshing frequency of the gear pair, φ_n is the phase angle, and a_n and b_n represents the expansion coefficients.

According to empirical formulas, the meshing damping of gear pairs can be expressed as [23]:

$$c_m = 2\xi_m \sqrt{k_p \frac{r_{bp}^2 r_{bg}^2 J_p J_g}{J_p r_{bp}^2 + J_g r_{bg}^2}} \tag{24}$$

where b_p and b_g represent the base circle radii of the driving and driven gears, and J_p and J_g are the rotational inertia of the driving and driven gears. ξ_m is the gear meshing damping ratio.

Assuming the backlash is $2b$, the nonlinear backlash function can be expressed as:

$$f(\delta) = \begin{cases} \delta - b, & \delta \geq b \\ 0, & -b < \delta < b \\ \delta + b, & \delta \leq -b \end{cases} \tag{25}$$

$$\delta = r_{bpk} \cdot \theta_{pk} - r_{bgk} \cdot \theta_{gk} - e(t) \tag{26}$$

where, r_{bpk} denotes the radius of the base circle of the corresponding pinion; r_{bgk} denotes the radius of the base circle of the corresponding large gear; θ_{pk} denotes the angular displacement of the corresponding pinion; θ_{gk} denotes the angular displacement of the corresponding large gear.

The meshing error is expressed in the form of Fourier series:

$$e(t) = e_0 + \sum_{i=1}^{n} e_i \cos(i\omega_n t + \varphi_{i0}) \tag{27}$$

where e_0 is the mean value of gear meshing error, e_i is the amplitude of the ith harmonic of the meshing error, ω_n means the meshing frequency, and φ_{i0} represents the initial phase angle of the ith harmonic.

4.2. Dynamic Response Analysis of the Gear Transmission

Due to the rigid connection between the motor and the input shaft of the reducer, the speed loss of the reducer can be ignored. The dynamic responses of the transmission system are analyzed. According to the rated power, rated torque and electromagnetic property of the motor, the input speed of the driving end n is set to 3280 r/min, and the input torque T_D is equal to 150 N·m. The variable step size Runge-Kutta method is adopted to solve the dynamic equations and obtain the dynamic responses of the transmission system.

Figure 8a illustrates the dynamic meshing force variations of the output stage gears over the time interval [4 s, 4.1 s]. As shown in Figure 8b, the excitation frequency components of the meshing force mainly include the meshing frequency and its multiples and the rotation frequency. The FFT spectrum peaks of the gear transmission located at the meshing frequency and its multiples and the rotation frequency modulation position. The dynamic meshing force has the most significant resonance peak at $2f_m + 3f_r$, and the amplitude at f_r is much smaller than the amplitude at f_m, close to the amplitude at $2f_m$. The excitation frequency is approximately the sum of the integer multiples of the meshing frequency and the integer multiples of the rotation frequency. Hence, these excitation frequencies are all harmonic frequencies and there are no noise frequencies and fault frequencies. The results indicate that the meshing processes are relatively stable.

In this study, Gear 1 will be used as a case for analysis. An analysis of the Poincaré sections presented in Figure 9 indicates that the motion cross-sections of Gear 1 in the x, y and z directions form closed curves, thereby implying that Gear 1 exhibits quasi-periodic motion during the meshing process. Furthermore, the acceleration change during the meshing process of Gear 1 can be fully represented in Figure 10. The acceleration change image displays periodicity, thus proving that Gear 1 carries out periodic vibratory motion in the x, y and z directions during the meshing process, and indirectly verifying the conclusions drawn from Figure 9.

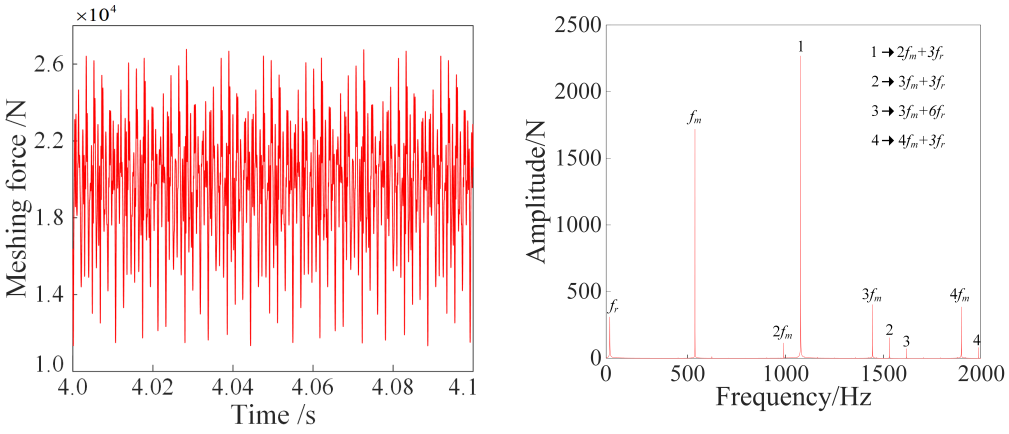

(**a**) DMF in time domain (**b**) DMF in frequency domain

Figure 8. Dynamic meshing forces of the output stage.

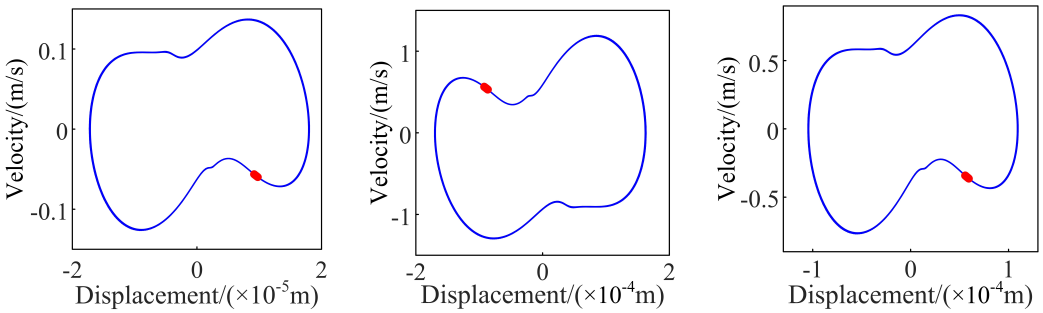

(**a**) *x*-direction (**b**) *y*-direction (**c**) *z*-direction

Figure 9. Poincaré section diagram of the gear 1.

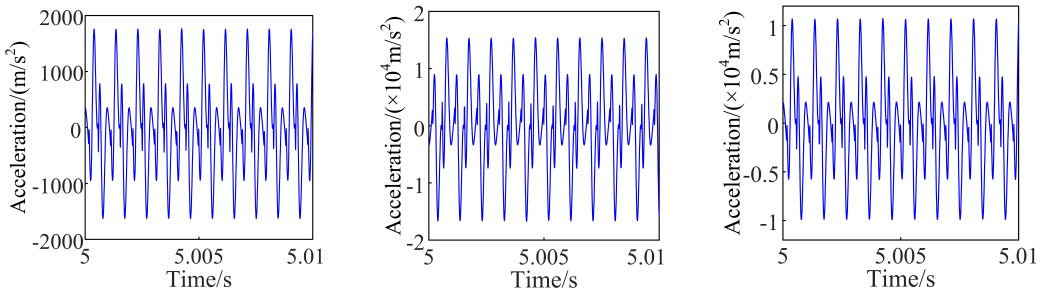

(**a**) *x*-direction (**b**) *y*-direction (**c**) *z*-direction

Figure 10. Vibration acceleration of the gear 1.

4.3. Effect of Mass Eccentricity on Dynamic Response

To investigate the effect of gear mass eccentricity on the dynamic response of gear meshing, the eccentricity data of the gear parameters after manual gear matching in Table 3 are adjusted. The mass eccentricity of four gears is tentatively set to be $\rho_1 = \rho_2 = \rho_3 = \rho_4 = 0.3$ mm, and under the same conditions of input power and torque, the backlash b is 1×10^{-5}m. Using the variable step size Runge-Kutta method to calculate the dynamic equation numerically, the dynamic responses of the transmission can be obtained as shown in Figures 11 and 12.

Table 3. Parameters for dynamic modeling of the gear transmission.

Name	Gear 1	Gear 2	Gear 3	Gear 4
m_i (kg)	1.16	5.84	1.32	9.61
k_{xi}, k_{yi}, k_{zi} (N/m)	6×10^8	1.5×10^7	1.5×10^7	1.5×10^7
c_{xi}, c_{yi}, c_{zi} (N·s/m)	3.54×10^4	3.85×10^3	3.85×10^3	3.85×10^3
k_{ei} (N/m)	$k_{e1} = 8 \times 10^8$	$k_{e2} = 1.5 \times 10^8$	$k_{e3} = 1.5 \times 10^8$	
c_{ei} (N·m·s/rad)	$c_{e1} = 1.47 \times 10^4$	$c_{e2} = 7.69 \times 10^4$	$c_{e3} = 7.69 \times 10^4$	
$J_D = 2.0 \times 10^7$ kg · m^2, $J_L = 5.0 \times 10^6$ kg · m^2, $e_r = 1.08 \times 10^{-4}$ m				

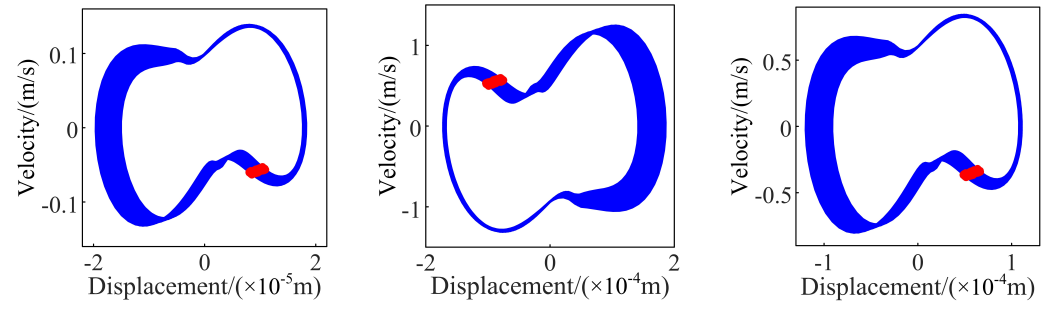

(**a**) *x*-direction (**b**) *y*-direction (**c**) *z*-direction

Figure 11. Poincaré section diagram of the gear 1 with mass eccentricity.

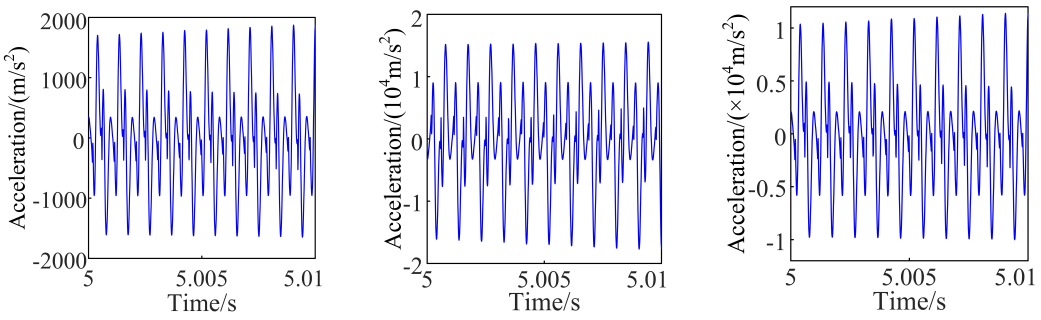

(**a**) x-direction (**b**) y-direction (**c**) z-direction

Figure 12. Vibration acceleration of the gear 1 with mass eccentricity.

As illustrated in Figure 11, the Poincaré section demonstrates that the motion section diagrams of Gear 1 in the x, y and z directions all form closed curves. Comparing Figure 10 with Figure 12, it can be found that the value of the gear vibration acceleration increases as the mass eccentricity increases, and the range of fluctuation tends to increase. Although gear 1 exhibits quasi-periodic motion during the meshing process, the closed curves display noticeable dispersion, indicating that the gear is transitioning from a quasi-periodic state to a chaotic one.

Figure 12 illustrates the variation in acceleration during the meshing process of Gear 1, thereby confirming that the acceleration range of the gear increases in conjunction with the rise in mass eccentricity. The periodicity of the acceleration variation remains unaltered, indicating that the periodicity of gear acceleration is largely unaffected. Comparing Figure 10 with Figure 12 reveals that there are differences in vibration acceleration between gears with and without mass eccentricity. A comparative analysis of the vibration acceleration signals of all gear teeth individually would be a rather complex undertaking, necessitating a quantitative presentation of the observed differences. It should be noted that parameters such as the standard deviation (σ), maximum value ($X_{\max}$), kurtosis (K_u), skewness (S_k) and clearance factor (CL_f) are susceptible to fluctuations in the signals under investigation. Therefore, it is necessary to investigate and compare these statistical parameters, which can be calculated using Equations (28)–(31).

$$\sigma = \sqrt{\frac{1}{n-1}\sum_{i=1}^{n}(x_i - \bar{x})^2} \tag{28}$$

$$Ku = \frac{\sum_{i=1}^{n}(x_i - \bar{x})^4}{n\sigma^4} \tag{29}$$

$$Sk = \frac{n}{(n-1)(n-2)}\sum_{i=1}^{n}\left(\frac{x_i - \bar{x}}{\sigma}\right)^3 \tag{30}$$

$$CL_f = \frac{X_{\max}}{X_r} \tag{31}$$

where, x_i represents the data of the signal, $\bar{x}$ represents the mean value of the signal, n represents the data number of the signal, $X_{\max}$ represents the maximum value of the signal, and X_r represents the square root value of the signal.

The mass eccentricity of four gears is tentatively set to be $\rho_1 = \rho_2 = \rho_3 = \rho_4$, with ρ_1 taking values in the range of $[0, 25\,\text{mm}]$ at intervals of 2.5 mm. The results of the variation of statistical parameters can be obtained as illustrated in Figure 13. Figure 13a illustrates the standard deviation of the vibration acceleration signals for Gear 1 as a function of increasing gear eccentricity. The curve exhibits notable fluctuations, reaching a maximum at a mass eccentricity of 10 mm. Similarly, Figure 13b–e present the maximum

values, kurtosis, skewness and clearance coefficients of the vibration acceleration signals for Gear 1 across the x, y and z directions. Each parameter shows a fluctuating trend, peaking in a specific range of mass eccentricity, and the standard deviation, maximum value, and skewness of the gear vibration acceleration vary relatively significantly. These findings indicate a significant correlation between the mass eccentricity of the gear and these five characteristic parameters, thereby demonstrating the feasibility of evaluating the degree of gear mass eccentricity based on the features of the acceleration vibration signals. Subsequent investigations can employ methods analogous to those discussed in Section 2.2, with a view to further evaluating the quality of the gear's mass eccentricity.

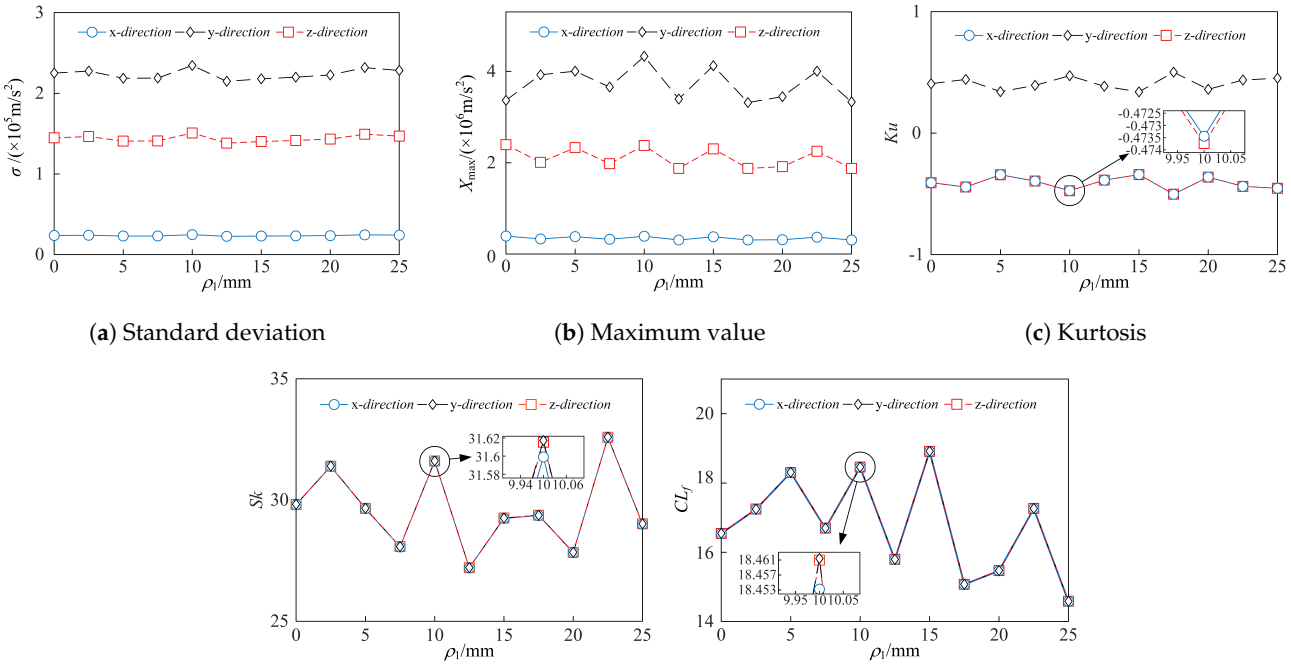

(**a**) Standard deviation (**b**) Maximum value (**c**) Kurtosis

(**d**) Skewness (**e**) Clearance factor

Figure 13. Variation of characteristic parameters of gear with changes in mass eccentricity.

5. Conclusions

A parameter-matching method based on fuzzy evaluation was proposed in this study. The geometric parameters of the gear transmission with the optimal transmission ratio are designed. The dynamic behaviour was analyzed to verify the design's feasibility. The main conclusions are obtained:

(1) This study employs fuzzy mathematics to develop a multidimensional evaluation model based on the power and economic performance of EVs. Using the gearbox ratio of a specific vehicle as a case study, the optimal ratio of 6.9 is identified for achieving comprehensive vehicle performance. This approach avoids the issue of local optimization caused by complex coupling relationships between performance parameters and streamlines the parameter matching process.

(2) A nonlinear dynamic model for helical gears is formulated, considering time-varying mesh stiffness, time-varying transmission error, the backlash and mass eccentricity. The dynamic response of the system is analyzed under the rated motor torque, revealing dynamic mesh force frequencies at multiples of the mesh and rotational frequencies. Smooth gear operation is indicated by the excitation frequency, with a maximum resonance peak observed at $2f_m + 3f_r$. The results demonstrate the model's effectiveness in accurately analyzing helical gear dynamics.

(3) The analysis of gear mass eccentricity's effect on dynamic response reveals a transition from quasi-periodic to chaotic motion as eccentricity increases. Characteristic parameter such as the standard deviation, maximum value, and skewness of vibration acceleration exhibit significant changes with varying mass eccentricity levels. These findings indicate the feasibility of inferring the degree of gear mass eccentricity based on vibrational characteristic parameters.

Author Contributions: Conceptualization, Y.G. and Y.L.; methodology, Y.L.; validation, Y.G. and Y.D.; formal analysis, Y.G. and G.N.; resources, Z.F.; data curation, Y.G.; writing—original draft preparation, Y.G. and Y.D.; writing—review and editing, Y.L. and Y.G.; visualization, Y.G. and G.N.; supervision, Z.F.; project administration, Y.L. and D.H.; funding acquisition, Y.L. All authors have read and agreed to the published version of the manuscript.

Funding: This study was funded by the National Natural Science Foundation of China (52405067), Hubei Provincial Natural Science Foundation of China (2023AFB066) and the Opening Foundation of Hubei Key Laboratory of Hydroelectric Machinery Design & Maintenance (2021KJX10).

Data Availability Statement: The original contributions presented in the study are included in the article, further inquiries can be directed to the corresponding authors.

Conflicts of Interest: Author Dong Huang was employed by the company Chongqing Tsingshan Industrial Co., Ltd. The remaining authors declare that the research was conducted in the absence of any commercial or financial relationships that could be construed as a potential conflict of interest.

References

1. Li, Z.; Khajepour, A.; Song, J. A comprehensive review of the key technologies for pure electric vehicles. *Energy* **2019**, *182*, 824–839. [CrossRef]
2. Jiang, F.; Yuan, X.; Hu, L.; Hu, L. A comprehensive review of energy storage technology development and application for pure electric vehicles. *J. Energy Storage* **2024**, *86*, 111159. [CrossRef]
3. Ifedi, C.; Mecrow, B.; Brockway, S.; Boast, G.; Atkinson, G.; Kostic-Perovic, D. Fault-tolerant in-wheel motor topologies for high-performance electric vehicles. *J. Energy Storage* **2013**, *49*, 1249–1257. [CrossRef]
4. Gao, S.; Zhang, Y.; Ji, S.; Liu, S.; Li, W. Double-stage multi-objective optimized design for cycloid pinwheel reducer based on genetic algorithm. *J. Mech. Sci. Technol.* **2024**, *38*, 333–345. [CrossRef]
5. Moya, J.; Gonzalez, E.; Moreno, E. Design of gear reducer for vehicle powered by in-wheel electric motor. *DYNA* **2022**, *97*, 374–379. [CrossRef]
6. Wang, S.; Xu, X.; Chen, X.; Li, R. Lightweight design of the planetary gear reducer of reduction drive hub motors. *J. Phys. Conf. Ser.* **2022**, *2338*, 012059. [CrossRef]
7. Zhao, Y.; Xu, X.; Han, Z.; Tan, Q.; Shan, W.; Li, R.; Wang, H.; Du, Y. Multi-Objective optimization design of cycloid-pin gears based on RV reducer precision transmission performance. *Energies* **2024**, *17*, 654. [CrossRef]
8. Marafona, J.; Carneiro, G.; Marques, P.; Martins, R.; Antônio, C.; Seabra, J. Gear design optimization: Stiffness versus dynamics. *Energies* **2024**, *191*, 105503. [CrossRef]
9. Hur, S.; Kim, D.; Lee, C.; Choi, D. Optimal design of a compound planetary reducer using a nonlinear optimization method. *IEEE Access* **2023**, *11*, 7822–7828. [CrossRef]
10. Trojovská, E.; Dehghani, M.; Trojovskỳ, P. Zebra optimization algorithm: A new bio-inspired optimization algorithm for solving optimization algorithm. *IEEE Access* **2022**, *10*, 49445–49473. [CrossRef]
11. Gao, H.; Zang, B.; Sun, L.; Chen, L. Evaluation of electric vehicle integrated charging safety state based on fuzzy neural network. *Appl. Sci.* **2022**, *12*, 461. [CrossRef]
12. He, S.; Wang, Y. Evaluating new energy vehicles by picture fuzzy sets based on sentiment analysis from online reviews. *Artif. Intell. Rev.* **2023**, *56*, 2171–2192. [CrossRef]
13. Khabou, M.; Bouchaala, N.; Chaari, F.; Fakhfakh, T.; Haddar, M. Study of a spur gear dynamic behavior in transient regime. *Mech. Syst. Signal Process.* **2011**, *25*, 3089–3101. [CrossRef]
14. Lin, C.; Sun, S.; Walker, P.; Zhang, N. Off-line optimization based active control of torsional oscillation for electric vehicle drivetrain. *Appl. Sci.* **2017**, *7*, 1261. [CrossRef]
15. Guo, D.; Zhou, Y.; Hu, M.; Li, M.; Li, Y.; Zhang, Z.; Rao, W. Analysis and optimization of tip-out transient dynamic characteristics of electric vehicle reducer under multi-bearing collaborative preloading. *Proc. Inst. Mech. Eng. Part D J. Automob. Eng.* **2024**, *238*, 3721–3735. [CrossRef]

16. Al-Tayari, A.; Chen, S.; Sun, Z. A coupled torsional-transition nonlinear vibration and dynamic model of a two-stage helical gearbox reducer for electric vehicles. *Shock Vib.* **2020**, *2020*, 8838521. [CrossRef]
17. Yan, M.; Liu, H. A dynamic modeling method for helical gear systems. *Shock Vib.* **2017**, *19*, 111–124. [CrossRef]
18. Chen, Z.; Ning, J.; Wang, K.; Zhai, W. An improved dynamic model of spur gear transmission considering coupling effect between gear neighboring teeth. *Nonlinear Dyn.* **2021**, *106*, 339–357. [CrossRef]
19. Kong, X.; Hu, Z.; Tang, J.; Chen, S.; Wang, Z. Effects of gear flexibility on the dynamic characteristics of spur and helical gear system. *Mech. Syst. Signal Process.* **2023**, *184*, 109691. [CrossRef]
20. Huang, K.; Cheng, Z.; Xiong, Y.; Han, G.; Li, L. Bifurcation and chaos analysis of a spur gear pair system with fractal gear backlash. *Chaos Solitons Fractals* **2021**, *142*, 110387. [CrossRef]
21. Guan, X.; Tang, J.; Hu, Z.; Wang, Q.; Kong, X. A new dynamic model of light-weight spur gear transmission systemconsidering the elasticity of the shaft and gear body. *Mech. Mach. Theory* **2022**, *170*, 104689. [CrossRef]
22. Zhang, Y.; Yuan, W.; Fu, R.; Wang, C. Design of an energy-saving driving strategy for electric buses. *IEEE Access* **2019**, *7*, 157693–157706. [CrossRef]
23. Hu, J.; Peng, T.; Jia, M.; Yang, Y.; Guan, Y. Study on electromechanical coupling characteristics of an integrated electric drive system for electric vehicle. *IEEE Access* **2019**, *7*, 166493–166508. [CrossRef]

Disclaimer/Publisher's Note: The statements, opinions and data contained in all publications are solely those of the individual author(s) and contributor(s) and not of MDPI and/or the editor(s). MDPI and/or the editor(s) disclaim responsibility for any injury to people or property resulting from any ideas, methods, instructions or products referred to in the content.